

## NUMERICAL STUDY OF TURBULENT MIXED CONVECTION OF AIRFLOW IN A ROOM USING REYNOLDS STRESS MODEL

Lincoln Batista, [lincoln\\_engmec@yahoo.com.br](mailto:lincoln_engmec@yahoo.com.br)  
Kátia Cordeiro Mendonça, [k.mendonca@pucpr.br](mailto:k.mendonca@pucpr.br)  
Viviana Cocco Mariani, [viviana.mariani@pucpr.br](mailto:viviana.mariani@pucpr.br)

Programa de Pós-Graduação em Engenharia Mecânica  
Pontifícia Universidade Católica do Paraná – PUCPR

**Abstract.** *This paper reports an experimentally validated numerical analysis of airflow through a non-isothermal three-dimensional room, where the air is supplied horizontally on the upper left and is exhausted through the opening located on the lower right. The dimensions of the room take the following values: height  $H = 3.0$  m, length  $L = 9.0$  m, width  $W = 14.1$  m, inlet height  $h = 0.168$  m, outlet height  $t = 0.48$  m, with the inlet and outlet openings as large as the room. The main purpose of the study is to assess the buoyancy and inertial forces effects at the airflow. Due to the turbulent flow, a Reynolds-stress model has been employed to predict the airflow pattern in the room. The model has been validated by comparing the numerical results with experimental data from the literature for dimensionless temperature and mean air velocities distributions on different regions of the room. The velocity vectors results have shown that the airflow pattern is significantly affected by increasing Archimedes number, and depends on the initial conditions when the buoyancy force predominates. In addition, the comparison between predictions from the turbulence model analyzed against those from the standard  $k-\varepsilon$  model has shown evidence that, for high buoyancy effects, different turbulence models can lead to different airflow patterns.*

**Keywords:** *turbulence, Reynolds-stress model, mixed convection, airflow.*

### 1. INTRODUCTION

Considerable success has been achieved by using the computational fluid dynamics (CFD) to predict indoor airflow, although there are still some difficulties as related in Chen (1995; 1996). The CFD to solve turbulent flow is further divided into three approaches types: direct numerical simulation (DNS), Reynolds Averaged Navier-Stokes (RANS) equation modeling, and large eddy simulation (LES). As the  $k-\varepsilon$  model assumes the isotropy for turbulence, anisotropic models such as RSM and LES are being recommended for the simulation of complex three-dimensional flows (Chen, 1996; Monokrousos *et al.*, 2008). However, RSM has deficiencies such as: non-universal model parameters, numerical difficulties, and it is computationally expensive by an order of magnitude when compared to the  $k-\varepsilon$  model.

Numerical simulations of mixed convection are available in literature. Nielsen *et al.* (1979) used the standard  $k-\varepsilon$  model with wall functions and calculated the flows in a ventilated room with a heated floor. The prediction agreed well with the experimental data, nevertheless it is known that the wall functions cannot calculate buoyancy effects accurately. Chen (1995) compared the performance of several  $k-\varepsilon$  models on indoor airflow simulation and found the performance of RNG  $k-\varepsilon$  model is better in mixed convection than in forced convection flows. The Reynolds stress model (RSM) was applied by Chen (1996) on indoor airflow simulations, and the performance of this model is less satisfactory in mixed convection than in forced and natural convection. The model combining a near-wall one-equation model and a near-wall natural convection model with the aid of direct numerical simulation (DNS) was investigated by Xu and Chen (2001), while the model using one-equation model for near-wall region and the standard  $k-\varepsilon$  model for the outer wall region was investigated by that authors for predicting forced, natural and mixed convection. Susin *et al.* (2009) investigated the influence of two values of inlet slot width on the velocity characteristics and turbulent intensity of the airflow inside an isothermal rectangular room. The performance of three turbulence models, standard  $k-\varepsilon$ , RNG  $k-\varepsilon$ , and  $k-\omega$  has also been investigated. On the whole, the performance of the standard  $k-\varepsilon$  model was better than those of the other two turbulence models. Mazzaro *et al.* (2010) studied the isotherm airflow in a room using two turbulence models, the standard  $k-\varepsilon$  and a RSM model, considering two aspect ratios of the room and two inlet slot widths. In general, both models gave similar velocity profiles. However, in terms of streamlines, the RSM model estimated more flow secondary recirculation than the standard  $k-\varepsilon$  model.

Direct numerical simulations have provided physical insight into the phenomena of transitional and turbulent flows, despite the fact that they are limited to simple and moderate Reynolds number flows (Moin and Mahesh, 1998). The fine grids (and the corresponding small time steps) necessary in the DNS of turbulent flows at moderate to high Reynolds numbers give rise to very high computational costs. Therefore, other approaches based on LES have been developed to be able to simulate transitional and turbulent flows in large-enough domains and at high Reynolds numbers. In LES the mesh size is chosen considerably larger than for DNS. For flows with solid walls, the thin boundary layers adjacent to the walls need to be resolved in both DNS and LES for accurate results. Therefore, even LES requires a substantial computational effort, but lower than DNS: A typical resolution for an LES is approximately 1–20% of a corresponding fully-resolved DNS (Monokrousos *et al.*, 2008).

From a practical point of view, the use of LES and DNS is still far from to be used commonly due to the high computational costs associated with them. For these reasons, it is thought that the RANS equations associated with turbulence modeling will be the main CFD tool used by researchers at least in the near future (Murthy and Joshi, 2008). Nevertheless, there is a need to improve the accuracy and reliability of the solutions of turbulent flow fields obtained from the RANS equations, selecting the model parameters on the basis of the understanding of mean and the turbulent flow fields. It is desirable that a benchmark database to be available with extensive exercises of the comparative performance of these turbulence models. Therefore, one of the objectives of the present study is to study the performance of the model RSM-LLR (Launder *et al.*, 1975) to predict the non-isothermal flow inside a well-known configuration, the Annex 20 test room (Nielsen, 1990). A second and main objective is to evaluate the influence of Archimedes numbers on the studied flow.

The remainder of the paper is organized as follows. The experimental apparatus (Nielsen, 1976) and physical problem are described in Section 2. In the same section, the governing equations and turbulence models are detailed, while the numerical methodology is introduced in Section 3. The main results concerning the turbulence model performance in predicting the indoor airflow are presented in Section 4. First, the focus is on the validation of the RSM-LLR model while in the second part a feedback about influence of Archimedes number on the referred flow is considered. The paper ends with a summary of the main conclusions.

## 2. PHYSICAL PROBLEM

The non-isothermal airflow regarding the Annex 20 benchmark described in Nielsen (1990), for which some experimental and numerical data are available in the current literature, was chosen to perform the proposed analysis. Nielsen's experiment was conducted in a cavity as shown in Figure 1. The floor is heated, and the air is supplied horizontally on the upper left by a rectangular opening and is exhausted through another rectangular opening located in the lower right of the room. Although the configuration is a laboratory model rather than an actual room, the flow is mixed convection and represents flow features found in real rooms.



Figure 1. Experimental apparatus (Nielsen, 1976), source: <http://www.cfd-benchmarks.com>.

Figure 2 shows a sketch of the numerical domain corresponding to the Nielsen's device with the dimensions recommend by Annex 20 as a benchmark exercise: height  $H = 3.0$  m, length  $L = 3.0H$ , width  $W = 4.7H$ , inlet height  $h = 0.056H$ , inlet width  $w = W$  and outlet height  $t = 0.16H$ . Experimental results for this flow are available in terms of dimensionless temperature profiles along two horizontal lines of the plane  $z/W = 0.66$ , at the floor ( $y = 0$ ) and at  $y = 0.75H$ , as illustrated in Figure 2.

This non-isothermal airflow is characterized by Reynolds and Archimedes numbers based on the height of the air inlet,  $Re = U_0 h / \nu$ , and on the difference of air temperature between the inlet and the outlet openings,  $Ar = \beta g h \Delta T / U_0^2$ , where  $U_0$  is the  $x$  direction mean velocity component in the inlet of the room [m/s],  $\nu$  is the kinematic viscosity [m<sup>2</sup>/s],  $\beta$  is the thermal expansion coefficient of air [1/K] and  $\Delta T$  is the difference of temperature between return and supply openings [K]. In the present work, seven cases have been considered as described in Table 1. The two first cases were established to validate the turbulence model under analysis, whereas the other cases (3<sup>rd</sup> to 7<sup>th</sup>) had been investigated to study the Archimedes effects on the fluid flow.

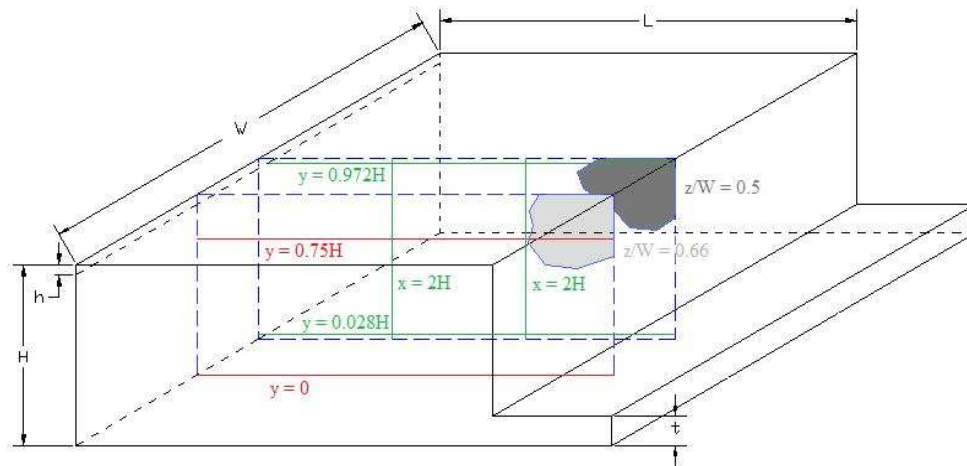


Figure 2. Sketch of the geometry studied.

Table 1. Configurations investigated in this study.

Case	Re	Ar	Floor heat flux (W/m <sup>2</sup> )
1	7,100	$1.10 \times 10^{-6}$	0.001156
2	2,400	$8.50 \times 10^{-5}$	0.003452
3	5,000	$1.10 \times 10^{-6}$	0.000367
4	5,000	$1.10 \times 10^{-4}$	0.036718
5	5,000	$1.10 \times 10^{-2}$	3.671821
6	5,000	$2.00 \times 10^{-1}$	73.436425
7	5,000	$1.73 \times 10^{-1}$	63.522508

### 3. PROBLEM FORMULATION

#### 3.1. Mathematical equations

Reynolds (1895) decomposed the Navier-Stokes equations in two parties, one related to the average value of the velocity vector and another related to its fluctuation, and applied the time average operator on them to study turbulent flows. The resulting set of equations is known as the Reynolds average Navier-Stokes (RANS) equations and gives information about the mean flow. Although this approach is not able to describe the multitude of length scales involved in turbulence, it has been largely used all of the world because in many engineering applications the information about the mean flow is quite satisfactory.

Considering that density and viscosity variations are small so that their effects on turbulence can be ignored, the fluid is Newtonian, the flow is incompressible and the steady state, the governing RANS equations in Cartesian coordinates can be expressed (Versteeg and Malalasekera, 1995) as:

$$\frac{\partial U_i}{\partial x_i} = 0, \quad (1)$$

$$\rho \frac{\partial (U_i U_j)}{\partial x_j} = -\frac{\partial P}{\partial x_i} + \frac{\partial}{\partial x_j} \left( \mu \frac{\partial U_i}{\partial x_j} - \overline{\rho u_i u_j} \right) + F_i, \quad (2)$$

where  $U_i$  and  $U_j$  are components of the average velocity vector [m/s],  $\rho$  is the fluid density [kg/m<sup>3</sup>],  $\mu$  is the dynamic viscosity of the fluid [Pa.s],  $P$  is the mean average pressure [Pa] and  $F_i$  is a component of the bulk force vector [N]. The extra-term that appears in Eq. (2) comparing to the original Navier-Stokes equations,  $\overline{u_i u_j}$ , is the product of fluctuation velocities [m<sup>2</sup>/s<sup>2</sup>] termed Reynolds stresses and is never negligible in any turbulent flow. It represents the increase in the diffusion of the mean flow due to the turbulence. Equations (1) and (2) can only be solved if the Reynolds stress tensor are known, a problem referred to as the 'closure problem' since the number of unknowns is greater than the number of equations.

The main goal of the turbulence studies based on RANS equations is therefore to determine the Reynolds stresses. According to Kolmogorov (1942) they can be evaluated by the following expression:

$$-\overline{u_i u_j} = \nu_t \left( \frac{\partial U_i}{\partial x_j} + \frac{\partial U_j}{\partial x_i} \right) - \frac{2}{3} \delta_{ij} k, \quad (3)$$

where  $\delta_{ij}$  is the Kronecker delta and the kinetic energy of the turbulent motion,  $k$ , is defined as  $k = \overline{u_i u_i} / 2$  [ $\text{m}^2/\text{s}^2$ ]. Substitution of Eq. (3) into Eq. (2) results in the average Navier-Stokes equations with the Reynolds stresses modeled via the viscosity concept,

$$\rho \frac{\partial(U_i U_j)}{\partial x_j} = -\frac{\partial P'}{\partial x_i} + \frac{\partial}{\partial x_j} \left[ (\mu + \mu_t) \left( \frac{\partial U_i}{\partial x_j} + \frac{\partial U_j}{\partial x_i} \right) \right] + \rho \beta (T_0 - T) g_i \quad (4)$$

where  $\mu_t$  is the turbulent viscosity,  $P' = P + 2/3k$  is the modified pressure,  $T_0$  is the temperature in a reference point [K],  $T$  is the temperature [K], and  $g$  is the gravity acceleration [ $\text{m}/\text{s}^2$ ]. The last term on the right side of Eq. (4) takes into account of buoyancy effects.

The turbulent viscosity can be expressed as the product of a velocity scale,  $u$  [m/s], and a length scale,  $L_\mu$  [m],  $\mu_t = \rho u L_\mu$ . Considering the velocity scale being calculated by  $u = k^{1/2}$ , Kolmogorov (1942) and Prandtl (1925) independently proposed the following relation for the turbulent viscosity,

$$\mu_t = \rho c_\mu k^{1/2} L_\mu, \quad (5)$$

where  $c_\mu (=0.09)$  is an empiric constant.

The momentum equation, Eq. (4), is coupled to the energy equation by the buoyancy term, and also by thermodynamics properties and transport coefficients if they are temperature dependent. As a result, the conservation of energy, Eq. (6), must be solved to obtain both temperature and velocity fields,

$$\frac{\partial(U_j T)}{\partial x_j} = \frac{\partial}{\partial x_j} \left[ \tau_{T,eff} \frac{\partial T}{\partial x_j} \right] + \dot{q} / \rho C_p, \quad (6)$$

where  $\tau_{T,eff}$  is the effective turbulent diffusion coefficient for Temperature [ $\text{m}^2/\text{s}$ ],  $\dot{q}$  is the thermal source [ $\text{W}/\text{m}^3$ ], and  $C_p$  is the specific heat at constant pressure [ $\text{J}/\text{kgK}$ ].

In order to complete the set of equations described above, the most popular turbulence models define two other transport equations: one for the turbulent kinetic energy,  $k$ , and another for a variable that relates  $k$  to  $L_\mu$ . These models are called two equations models, and the standard  $k$ - $\varepsilon$  model (Launder and Spalding, 1974) was tested in this study with the explicit formulations described below.

In the standard  $k$ - $\varepsilon$  model, proposed by Launder and Spalding (1974), the second variable for the complementary transport equations is the rate of the viscous dissipation,  $\varepsilon$  [ $\text{m}^2/\text{s}^3$ ], which is related to  $k$  by:

$$\varepsilon = k^{3/2} / L_\mu. \quad (7)$$

Consequently, the turbulent viscosity  $\nu_t$  is calculated in the  $k$ - $\varepsilon$  model as

$$\nu_t = c_\mu k^2 / \varepsilon. \quad (8)$$

The resulting set of equations concerning the standard  $k$ - $\varepsilon$  model is then composed of Eqs. (1), (4) and two transport equations for  $k$  and  $\varepsilon$  that are, respectively, given by:

$$\frac{\partial(U_j k)}{\partial x_j} = \frac{\partial}{\partial x_j} \left[ \left( \nu + \frac{\nu_t}{\sigma_k} \right) \frac{\partial k}{\partial x_j} \right] + \nu_t \left[ \frac{\partial U_i}{\partial x_j} + \frac{\partial U_j}{\partial x_i} \right] \left[ \frac{\partial U_i}{\partial x_j} \right] - \varepsilon, \quad (9)$$

$$\frac{\partial(U_j \varepsilon)}{\partial x_j} = \frac{\partial}{\partial x_j} \left[ \left( \nu + \frac{\nu_t}{\sigma_\varepsilon} \right) \frac{\partial \varepsilon}{\partial x_j} \right] + c_1 \nu_t \frac{\varepsilon}{k} \left[ \frac{\partial U_i}{\partial x_j} + \frac{\partial U_j}{\partial x_i} \right] \left[ \frac{\partial U_i}{\partial x_j} \right] - c_2 \frac{\varepsilon^2}{k}, \quad (10)$$

where  $c_1 = 1.42$  and  $c_2 = 1.92$  are empirical constants, and  $\sigma_k = 1$  and  $\sigma_\varepsilon = 1.22$  are turbulent Prandtl numbers.

The standard  $k$ - $\varepsilon$  model was developed for high Reynolds number flows; therefore it cannot represent adequately the viscous region near solid surfaces. This problem is solved coupling to the above-mentioned set of equations semi-empiric wall functions to represent the near-wall flow. Besides, the use of wall functions saves computing time because avoids the fine grid near the walls necessary in low Reynolds number models.

The Reynolds Stress Model (RSM) is based on transport equations of the Reynolds tensor and dissipation rate of turbulent kinetic energy. Solving a transport equation for each component of the Reynolds tensor the RSM add for a three-dimensional flow six new equations to the equations system. The RSM model is called a second moment closure due to model only terms of third or higher order. There are several variations of RSM, the model used in this study is known as RSM-LLR described in Launder *et al.* (1975). The transport equations for the Reynolds tensor are derived from the Navier-Stokes equations and are described by:

$$\rho \frac{\partial(U_j \tau_{ik})}{\partial x_j} = P_{ik} - \rho \varepsilon_{ik} + \frac{\partial}{\partial x_j} \left[ \nu \frac{\partial \tau_{ik}}{\partial x_j} + C_{ikj} \right] + \Pi_{ik}, \quad (11)$$

where the first term represents the variation rate of the viscous stress tensor,  $\tau$ , due to production,  $P$ , and dissipation of the turbulent kinetic energy,  $\varepsilon$ , the fourth term represents the molecular and turbulent diffusion, and the last term correlates pressure and tension.

The production, the dissipation of the turbulent kinetic energy, and the turbulent diffusion can be described by,

$$P_{ik} = - \left[ \tau_{ik} \frac{\partial U_k}{\partial x_j} + \tau_{ik} \frac{\partial U_i}{\partial x_j} \right], \quad (12)$$

$$\varepsilon_{ik} = \frac{2}{3} \varepsilon \delta_{ik}, \quad (13)$$

$$C_{ikj} = \overline{\rho u'_i u'_k u'_j} + \overline{p' u'_i \delta_{kj}} + \overline{p' u'_k \delta_{ij}}. \quad (14)$$

The last term in Eq. (11) combine the pressure with deformation of the flow, this term is responsible by redistribution of turbulent kinetic energy among the components of the Reynolds stress tensor, and can be described as:

$$\Pi_{ik} = \frac{p'}{\rho} \left( \frac{\partial u'_i}{\partial x_k} + \frac{\partial u'_k}{\partial x_i} \right). \quad (15)$$

In the RSM-LLR model used in this study, proposed by Launder *et al.* (1975), the Eq. (15) is described as:

$$\Pi_{ik} = -\rho \varepsilon C_1 a + C_2 \rho k S + C_4 \rho k (a S^T + S a^T - 2a \cdot S \delta / 3) + C_5 \rho k (aa + W a^T)], \quad (16)$$

where  $a = u_i / k - 2\delta / 3$  is the anisotropy tensor,  $S = [\bar{\nabla} U + (\bar{\nabla} U)^T] / 2$  is the tensor rate,  $W = [\bar{\nabla} U - (\bar{\nabla} U)^T] / 2$  is the vorticity,  $C_1 = 1.8$ ,  $C_2 = 0.8$ ,  $C_4 = C_5 = 0.6$  are constants.

### 3.2. Boundary Conditions

The inlet boundary conditions for velocity components were specified as  $U = U_0$  and  $V = W = 0$ , respectively, with  $U_0$  being the air average velocity in the inlet of the cavity obtained from Reynolds number based on the inlet height,  $Re = U_0 h / \nu$ , equals to 2,400; 5,000 and 7,100 as the case specified in Table 1. Regarding  $k$  and  $\varepsilon$ , the inlet boundary conditions were calculated by  $k_0 = 1.5(0.04 U_0)^2$  and  $\varepsilon_0 = 10 k^{3/2} / h$ , respectively. Zero relative pressure and zero gradients for the other variables are applied as the boundary conditions for the outlet. At the solid boundaries the no-slip and the impermeable wall boundary conditions were imposed for the velocity components, that is,  $U = V = W = 0$ . The turbulence quantities  $k$ , and  $\varepsilon$  are nulls at the walls. With the exception of the floor, along which a constant heat flux was added, please refer to Table 1, all walls were assumed adiabatic.

## 4. NUMERICAL APPROACH

The numerical solution of the governing equations was performed using the commercial computational fluid dynamics code Ansys CFX version 11. In this code the conservation equations for mass, momentum and turbulence quantities are solved using the finite volume discretization method generated by staggered grids.

In the method adopted in this work the interpolation of the properties at the control volume faces can be of primary importance on the accuracy of the numerical results. The classical approach of first order accurate upwind differencing usually suffers from inaccuracies in simulating complex flow situations. An effective approach to reduce truncation error, while maintaining the grid size within computational resource limits, is the adoption of a more accurate differencing scheme into the numerical analysis. In the present work, the first order upwind difference scheme (UDS) is firstly adopted in the solution of the governing equations, after that, such values are used to initialize the high resolution scheme (HRS). The HRS is both, accurate, reducing to first order near discontinuities and in the free stream where the solution has little variation, and bounded. Therefore its order of accuracy for the interpolated values can be major that two. The solution was considered converged when the sum of absolute normalized residuals for all cells in the flow domain becomes less than  $10^{-6}$ .

## 5. RESULTS AND DISCUSSION

The present study was conducted in three parts. Firstly, the influence of the spatial structured discretization on the prediction of the airflow was investigated, allowing to determining a grid independent solution for the turbulence model under analysis. Secondly, the effects of buoyancy and inertia forces have been analyzed by comparing the airflow pattern obtained by the RSM-LLR model for different Archimedes numbers. Lastly, by means of streamlines, the predictions from the RSM-LLR model have been confronted to those from the standard  $k-\epsilon$  model.

### 5.1. Analyzing the influence of grid refinement

The grid independent solution for the turbulence model tested was defined by comparing the computed results for  $Re = 7,100$  and  $Ar = 1.1 \times 10^{-6}$  (case 1) and  $Re = 2,400$  and  $Ar = 8.5 \times 10^{-5}$  (case 2) using different grid schemes with those available from Nielsen's experiment (Nielsen, 1976). As indicated in Fig. 2, dimensionless temperature profiles are available along two horizontal lines of the plane  $z/W=0.66$ , at  $y = 0$  and  $y = 0.75H$ . Since both cases represent low buoyancy effects, their results in terms of dimensionless mean velocity profiles have also been compared to the experimental data from the Annex 20 isothermal case (Nielsen, 1990) to complete the grid-dependency analysis.

In each grid the refinement was mainly carried out next to the walls, where the flow property gradients are steeper, considering the limit values of  $y^+$  for the wall function. According to the Ansys CFX version 11 manual, the range of  $y^+$  for the RSM-LLR model is  $20 < y^+ < 100$ . Table 2 shows the resulting grid schemes for case 2 disregarding the region after the outlet slot (see Fig. 2), which correspond to the following number of nodes: Grid 1 (13,125 nodes), Grid 2 (52,500 nodes) and Grid 3 (210,000 nodes)

Table 2. Number of nodes in directions x, y and z employed in each grid tested.

	Total volumes	Re = 2,400 and Ar = $8.5 \times 10^{-5}$		
		x	y	z
Grid 1	13,125	25	21	25
Grid 2	52,500	25	42	50
Grid 3	210,000	50	84	50

The deviations between the calculated dimensionless velocity and temperature values obtained with the different grids were determined by the root mean square error given by:

$$RMSE = \sqrt{\frac{1}{n} \sum_{i=1}^n (X_i^p - X_i^m)^2} \quad (17)$$

where  $X^p = (T - T_0)/\Delta T_0$  or  $U/U_0$  are the predicted dimensionless temperature or horizontal velocity,  $X^m$  are the measured dimensionless temperature or horizontal velocity, and  $n$  is the number of elements in the sample.

The comparisons between dimensionless temperature and horizontal velocity profiles are presented in this paper only for  $Re = 2,400$  and  $Ar = 8.5 \times 10^{-5}$  (Figs. 3 and 4, respectively), because the behavior of case 1 is similar to that of case 2. Note that the results of grid 3 agree satisfactorily with the experimental data, mainly to velocities at the central plane however some minor differences occur to temperature at plane  $z/W = 0.66$ .

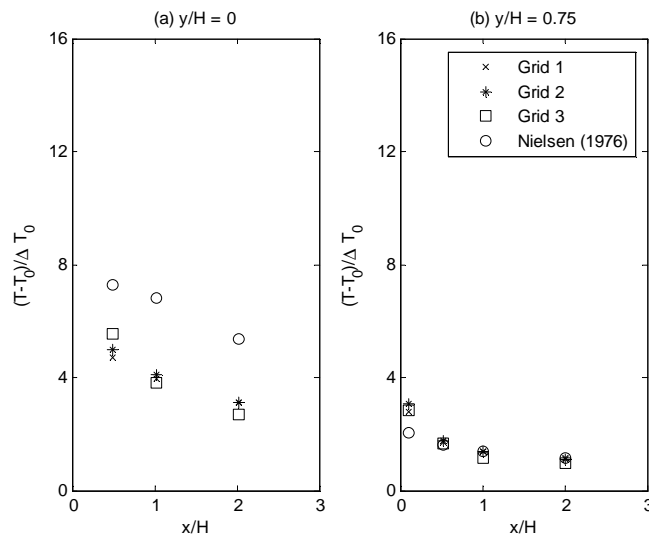


Figure 3. Effect of grid size on dimensionless temperature distributions at lines (a)  $y = 0$  and (b)  $y = 0.75H$  of plane  $z/W=0.66$  for  $Re = 2,400$  and  $Ar = 8.5 \times 10^{-5}$  (case 2).

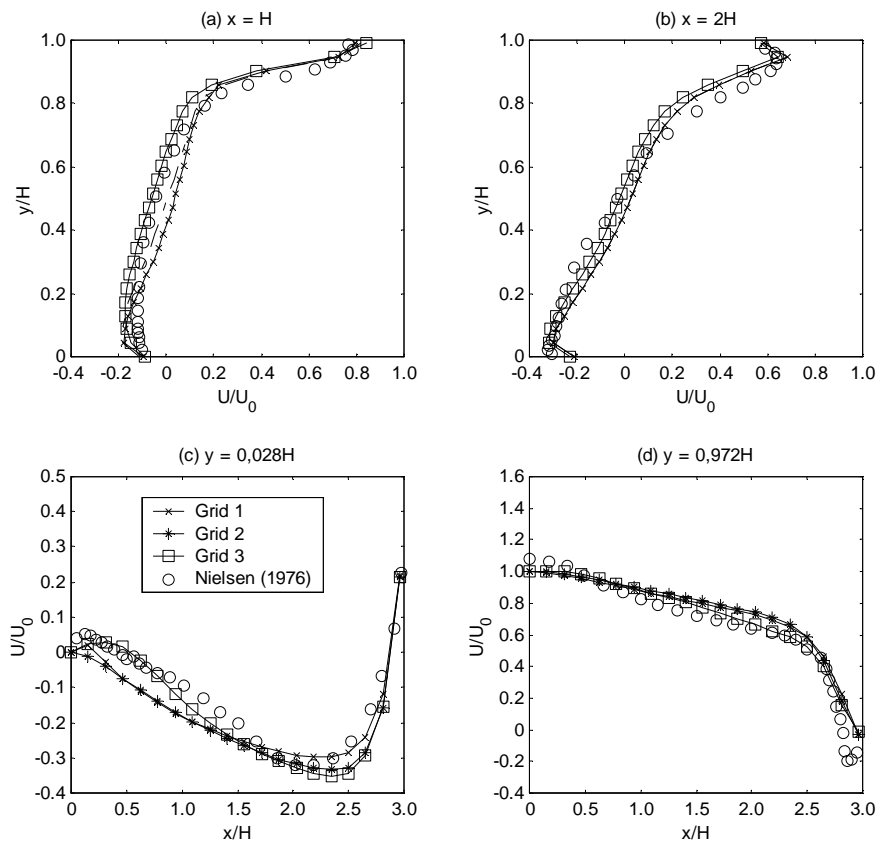


Figure 4. Effect of grid size on dimensionless velocity distribution at lines  $x = H$ ,  $x = 2H$ ,  $y = 0.028H$  and  $y = 0.972H$  of central plane for  $Re = 2,400$  and  $Ar = 85 \times 10^{-6}$  (case 2).

Table 3 describes the RMSE calculated for each computational grid used with RSM-LRR turbulence model in six different positions of two planes of the room. According Table 3, Grid 3 provided the smallest average RMSE value and reduced computational time consequently it was the grid chosen for the other simulations.

Table 3. Root mean square errors based on dimensionless horizontal velocity and temperature values for case 2.

Grid	Velocity	Temperature	Running
	Plane $z/W = 0.5$	Plane $z/W = 0.66$	time
	Average	Average	Hours
1	0.0869	1.469	12.45
2	0.0820	1.473	20.82
3	0.0749	1.470	38.10

### 5.2. Analyzing the influence of buoyancy and inertial forces effects

The influence of the buoyancy phenomenon on the airflow behavior has been assessed by comparing the changes in the airflow pattern with the increase of the importance of the heat transfer on the floor, as indicated in Fig. 5 by means of the predicted velocity vectors in the central plane of the studied geometry.

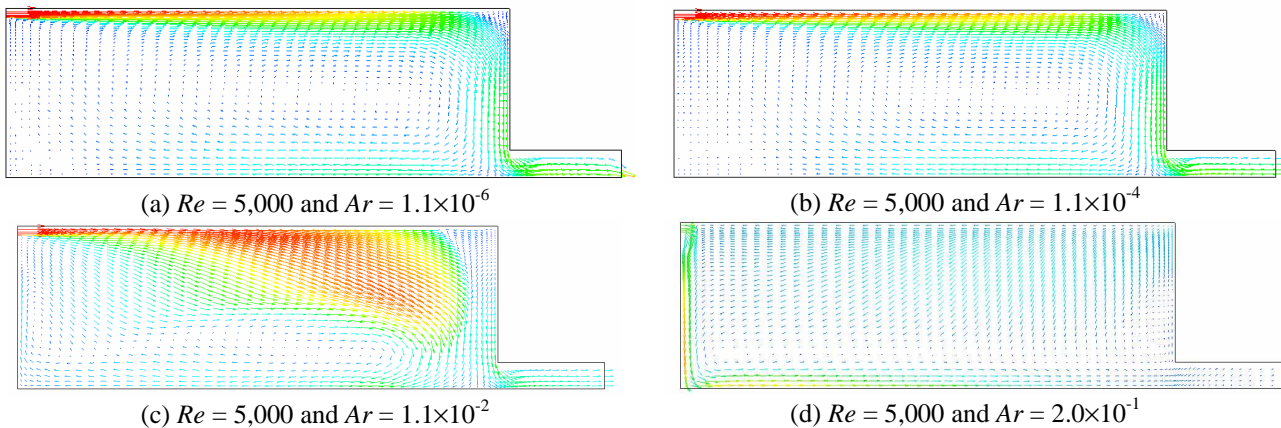
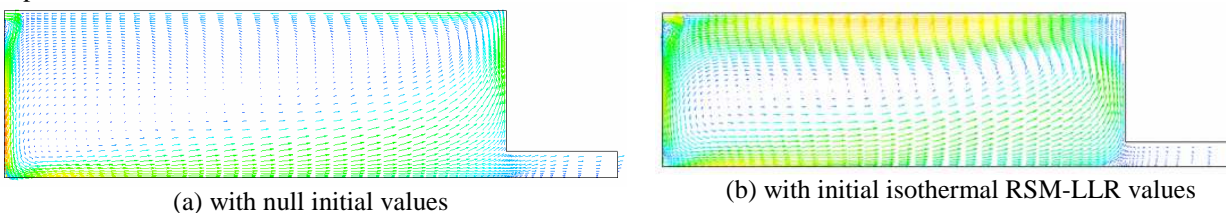


Figure 5. Velocity vectors in the central plane of the room predicted by the RSM-LLR model for different buoyancy effects.

It can be noted, from Fig. 5, important changes in the movement of the fluid at the central plane of the room as the Archimedes number has been gradually raised from  $1.0 \times 10^{-6}$  to  $2.0 \times 10^{-1}$ , while the Reynolds number has been maintained constant and equals to 5,000. At first, the flow pattern is similar to that found for the isothermal case (see Susin *et al.*, 2009); the jet develops along the ceiling and creates a main recirculation zone dislocated to the right side of the room, Figs. 5a and 5b, which indicates that inertial forces is the predominant one. In the next case, with an Archimedes number equals to  $1.0 \times 10^{-2}$  (Fig. 5c), the jet starts flowing attached to the ceiling and then drops into the occupied zone with high velocities. The main recirculation is dislocated to near the floor, and a second recirculation zone can be observed on the down left corner of the room. A predominant phenomenon cannot be distinguished. The last case, Fig. 5d, shows a very different behavior of the airflow within the room. Since the difference of temperature between the supply air and that inside the room is important, the jet falls down as soon as it enters the room causing the inversion of the flow. The buoyancy is now the dominant effect.

As it has been observed by Lemaire (1991), the airflow pattern depends on the initial conditions when the buoyancy effects are strong. Hence, in Fig. 6 is presented a comparison between the velocity vectors in the central plane of the room calculated with different initial conditions for case 7,  $Re = 5,000$  and  $Ar = 1.73 \times 10^{-1}$ . The first three figures show the predictions using the RSM-LLR model, while the last one was obtained with the standard  $k-\epsilon$  model for comparative purposes.



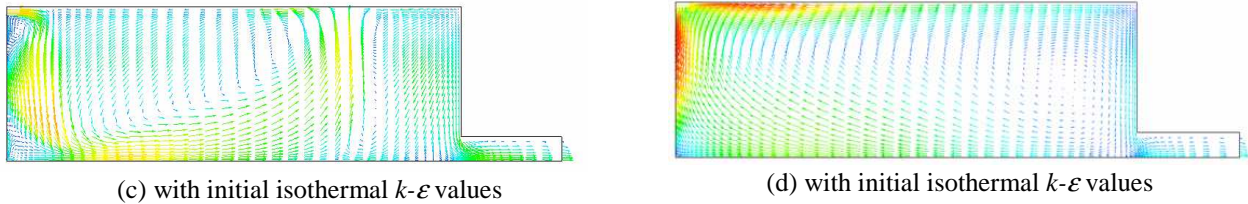


Figure 6. Influence of the initial values on the velocity vectors in the plane  $z/W = 0.5$  predicted by (a, b, c) RSM-LRR and (d) standard  $k-\epsilon$  models for case 7,  $Re = 5,000$  and  $Ar = 1.73 \times 10^{-1}$ .

When the initial conditions were nulls, the air movement inside the room was very close to that illustrated in Fig. 5d with  $Re = 5,000$  and  $Ar = 2.0 \times 10^{-1}$ , which was calculated using similar initial conditions. However, the predictions by the RSM-LLR model using the solution of the isothermal case have revealed a main recirculation zone dislocated to the left side of the room and also a region of quite high velocities next to the ceiling when the solution came from the RSM-LLR model itself (Fig. 6b), and the separation of the flow into two recirculation zones with different orientations (Fig. 6c) when it came from standard  $k-\epsilon$  model. The standard  $k-\epsilon$  model using initial conditions from the  $k-\epsilon$  model itself predicted an airflow pattern closer to the cases with low buoyancy effects, similar to airflow illustrated in Figs. 5a and 5b, the main recirculation is on the clockwise direction and dislocated to the right side of the room. But, in contrast to the low buoyancy cases, the jet region cannot be distinguished very well and high velocities are observed just below the inlet opening.

### 5.3. Comparing the predictions from RRS-LLR and standard $k-\epsilon$ models

Figure 7 shows the contours lines of the stream at the plane  $z/W = 0.5$  predicted by the RSM-LRR and standard  $k-\epsilon$  models for different buoyancy effects. For cases 3 and 4, where the inertia is the predominant force and the flow develops completely along the ceiling of the room, the airflow patterns predicted by both models are quite similar except for next to the left wall. In this region, the  $k-\epsilon$  model predicts an upward flow almost parallel to the left wall while the RSM-LRR model shows a secondary recirculation on the lower corner for case 3 (Fig. 7a) and a flow bended to the right side for case 4 (Fig. 7c). Comparing the separation point on the floor and the attachment point on the wall in this same region, note that such points are higher for the RSM-LRR model than for the  $k-\epsilon$  model in cases 3 and 4, whereas the throw of the jet is approximately the same for both turbulence models. With respect to the streamlines presented in Figs. 7e and 7f, it is possible to see that the airflow pattern obtained from each turbulence model is very different, there are variations in size, in position and in magnitude of the main recirculation zone. It can be inferred from this last comparison that not only when the buoyancy effect clearly predominates, as indicated by Figs. 6c e 6d, different turbulence models can conduct to different airflow patterns.

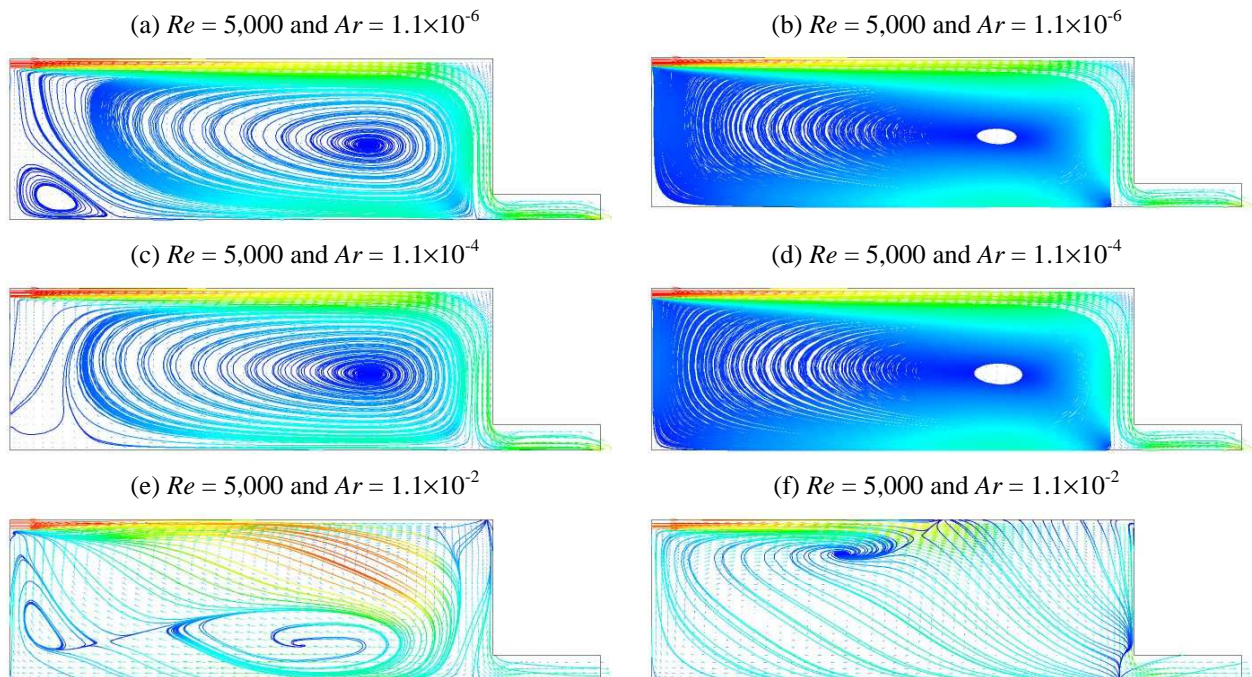


Figure 7. Streamlines for cases 3 to 5 predicted by (a, c, e) RSM-LRR and (b, d, f) by standard  $k-\epsilon$  models at the plane  $z/W = 0.5$ .

## 5. CONCLUSIONS

In this work, three-dimensional numerical simulations of turbulent airflow through a non-isothermal room were conducted for seven cases classified according the buoyancy effect. The airflow has been modeled using the Reynolds average Navier-Stokes equations and primarily a turbulence model of second order closure: the Reynolds Stress Model (RSM-LLR) proposed by Launder *et al.* (1975). For comparative purposes, some cases have also been simulated using the standard  $k-\varepsilon$  model (Launder and Spalding, 1974). The RSM-LLR model has been validated by comparing the numerical results with experimental data from the literature for dimensionless temperature and mean air velocities distributions on different regions of the room, considering three grid levels. The choice of the best grid occurred through the RSME evaluation. After the choice of the best grid, the influence of the buoyancy and inertial forces on the airflow pattern has been investigated. By analyzing the results of the seven cases, it has been observed significant differences between the cases in the level of the streamlines and velocity vectors with the increase of the buoyancy effect, even the inversion of the flow when the buoyancy force is the predominant one. Moreover, besides the influence of the initial conditions, the predictions show evidence of dependency on the turbulence model for the cases with high buoyancy effect. This is an ongoing project; therefore further analysis must be carried out in order to obtain more conclusive information about the influence of initial conditions and turbulence models on the airflow pattern.

## 6. ACKNOWLEDGEMENTS

The authors would like to thank CNPq (*Conselho Nacional de Desenvolvimento Científico e Tecnológico* - Brazil) (process 302786/2008-2/PQ) and Fundação Araucária for their financial support to this work.

## 7. REFERENCES

- Chen Q., 1995, "Comparison of different  $k-\varepsilon$  models for indoor air flow computations", Numerical Heat Transfer, Part B Vol. 28, pp. 353-369.
- Chen Q., 1996, "Prediction of room air motion by Reynolds-stress models", Building and Environment, Vol. 31, pp. 233-244.
- Kolmogorov A.N., 1942, "Equations of turbulent motion of an incompressible fluid". Izvestia Academy of Science, USSR, Physics, Vol. 6, No. 1-2, pp. 56-58.
- Launder B.E. and Spalding D.B., 1974, "The numerical computation of turbulent flows", Comp. Meth. Appl. Mech. Energy, pp. 269-289.
- Launder, B.E., Reece, G.J. and Rodin, W. 1975, "Progress in the developments of a Reynolds-stress turbulence closure". Journal of Fluid Mechanics, Vol. 68, pp. 537-566.
- Mazzaro, R.E., Mariani, V.C., Mendonça, K.C., 2010, "Performance of RSM turbulence model in predicting the airflow in a ventilated room", Proceedings of the 13<sup>th</sup> Brazilian Congress of Thermal Sciences and Engineering, Vol. 1, Uberlândia, Brazil, pp. 1-10.
- Moin, P. and Mahesh, K., 1998, "Numerical simulation: a tool in turbulence research". Annu. Rev. Fluid Mech., Vol. 30, pp. 539-578.
- Monokrousos, A., Brandt, L., Schlatter, P. and Henningson, D.S., 2008, "DNS and LES of estimation and control of transition in boundary layers subject to free-stream turbulence", International Journal of Heat and Fluid Flow, Vol. 29, pp. 841- 855.
- Murthy, B.N. and Joshi, J.B., 2008. "Assessment of standard  $k-\varepsilon$ , RSM and LES turbulence models in a baffled stirred vessel agitated by various impeller designs", Chemical Engineering Science, Vol. 63, pp. 5468 - 5495.
- Nielsen, P.V., 1976. "Flow in air conditioned rooms", (English translation of Ph.D. thesis, Technical University of Denmark, 1974), Danfos A/S, Denmark.
- Nielsen P.V., 1990. "Specification of a two-dimensional P.V. test case", Technical report, International Energy Agency, Annex 20: Air Flow Pattern Within Buildings.
- Nielsen P.V., Restivo A. and Whitelaw J.H., 1979, "Buoyancy-affected flows in ventilated rooms", Numerical Heat Transfer, Vol. 2, pp. 115-127.
- Prandtl L., 1925, "Über die ausgebildete turbulenz", ZAMM, Vol. 5, pp.136-139.
- Reynolds O., 1895. "On the dynamical theory of incompressible viscous fluids and the determination of the criterion", Phil. Trans. Roy. Soc. London Ser. A, Vol. 186, pp.123-164.
- Susin, R.M., Lindner, G.A., Mariani, V.C. and Mendonça, K.C., 2009, "Evaluating the influence of the width of inlet slot on the prediction of indoor airflow: comparison with experimental data", Building and Environment, Vol. 44, pp. 971-986.
- Versteeg H.K. and Malalasekera W., 1995. "An introduction to computational fluid dynamics", Longman Scientific & Technical, New York.
- Xu W. and Chen Q., 2001, "A two-layer turbulence model for simulation indoor airflow Part II". Applications, Energy and Buildings, Vol. 33, pp. 627-639.

## 8. RESPONSIBILITY NOTICE

The authors, Lincoln Batista, Kátia Cordeiro Mendonça and Viviana Cocco Mariani are the only responsible for the printed material included in this paper.